JACS
JOURNAL OF THE AMERICAN CHEMICAL SOCIETY

Article

pubs.acs.org/JACS

Stretchable Self-Healing Polymeric Dielectrics Cross-Linked Through Metal–Ligand Coordination

Ying-Li Rao,[†] Alex Chortos,[‡] Raphael Pfattner,[†] Franziska Lissel,[†] Yu-Cheng Chiu,[†] Vivian Feig,[‡] Jie Xu,[†] Tadanori Kurosawa,[†] Xiaodan Gu,[†] Chao Wang,[†] Mingqian He,[§] Jong Won Chung,[†,∥] and Zhenan Bao*[,†]

[†]Department of Chemical Engineering and [‡]Materials Science and Engineering Department, Stanford University, Stanford, California 94305, United States

[§]Corning Incorporated, SP-FR-06-1, Corning, New York 14831, United States

[∥]Samsung Advanced Institute of Technology Yeongtong-gu, Suwon-si, Gyeonggi-do 443-803, South Korea

Supporting Information

ABSTRACT: A self-healing dielectric elastomer is achieved by the incorporation of metal–ligand coordination as cross-linking sites in nonpolar polydimethylsiloxane (PDMS) polymers. The ligand is 2,2′-bipyridine-5,5′-dicarboxylic amide, while the metal salts investigated here are Fe^{2+} and Zn^{2+} with various counteranions. The kinetically labile coordination between Zn^{2+} and bipyridine endows the polymer fast self-healing ability at ambient condition. When integrated into organic field-effect transistors (OFETs) as gate dielectrics, transistors with $FeCl_2$ and $ZnCl_2$ salts cross-linked PDMS exhibited increased dielectric constants compared to PDMS and demonstrated hysteresis-free transfer characteristics, owing to the low ion conductivity in PDMS and the strong columbic interaction between metal cations and the small Cl^- anions which can prevent mobile anions drifting under gate bias. Fully stretchable transistors with $FeCl_2$-PDMS dielectrics were fabricated and exhibited ideal transfer characteristics. The gate leakage current remained low even after 1000 cycles at 100% strain. The mechanical robustness and stable electrical performance proved its suitability for applications in stretchable electronics. On the other hand, transistors with gate dielectrics containing large-sized anions (BF_4^-, ClO_4^-, $CF_3SO_3^-$) displayed prominent hysteresis due to mobile anions drifting under gate bias voltage. This work provides insights on future design of self-healing stretchable dielectric materials based on metal–ligand cross-linked polymers.

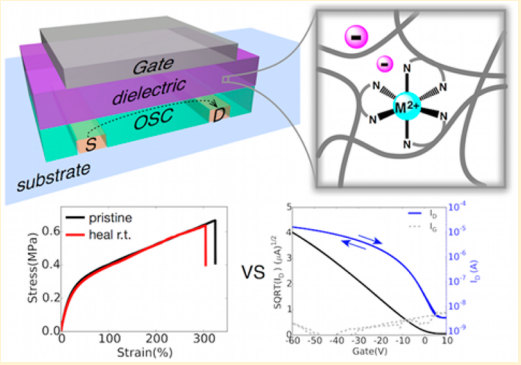

1. INTRODUCTION

Flexible electronics have generated tremendous interest among the scientific and engineering communities.[1−5] Due to their lightweight, flexibility, large-area printability,[6] and potential biodegradability,[7,8] organic-based flexible electronics hold great potential in applications such as wearable electronics[9] and medical devices.[10] Moreover, the ability to self-heal upon rupture or scratch can significantly improve the devices' lifetime. Various strategies have been applied to achieve organic self-healable conductors,[11] luminescent materials,[12] and battery electrodes.[13]

However, self-healing electronic materials still remain limited. For repeatable autonomous self-healing materials, the ability to restore their original mechanical properties upon damage relies on the incorporation of dynamic molecular bonds, namely stimuli-induced reversible bond breaking and reformation.[14] Dynamic molecular bonds are divided into two general categories: covalent adaptive bonds or supramolecular non-covalent bonds, such as hydrogen bonding, $\pi-\pi$ stacking, hydrophobic, host–guest complexation, metal–ligand coordination. Compared to other dynamic molecular bonds, metal–ligand coordination interactions are particularly attractive, as a broad range of molecular parameters, such as the identity of the metal ions, counterions, and ligands, can be varied to tune the bond strengths, endowing desirable material properties. A wide selection of dynamic metal–ligand interactions has been exploited in the literature for the development of self-healable materials. For example, Bielawski et al. showed a class of thermally healable organometallic conducting polymers comprising group 10 transition-metal salts (Ni, Pd and Pt) and N-heterocyclic carbenes.[15] Rowan, Weder, and co-workers reported photoactivated healable supramolecular polymers employing coordination between La^{3+}, Zn^{2+} metal ions and 2,6-bis(1-methylbenzimidazolyl)pyridine.[16] Holten-Andersen and co-workers prepared a self-healing gel containing Fe^{3+}-catechol coordinate bonds.[17] Guan et al. developed a hard/soft two-phase brush copolymer integrating Zn^{2+}-imidazole interactions in the soft matrix, which exhibited autonomous self-healing ability at room temperature.[18] Our group has recently

Received: March 10, 2016
Published: April 21, 2016

DOI: 10.1021/jacs.6b02428
J. Am. Chem. Soc. 2016, 138, 6020–6027

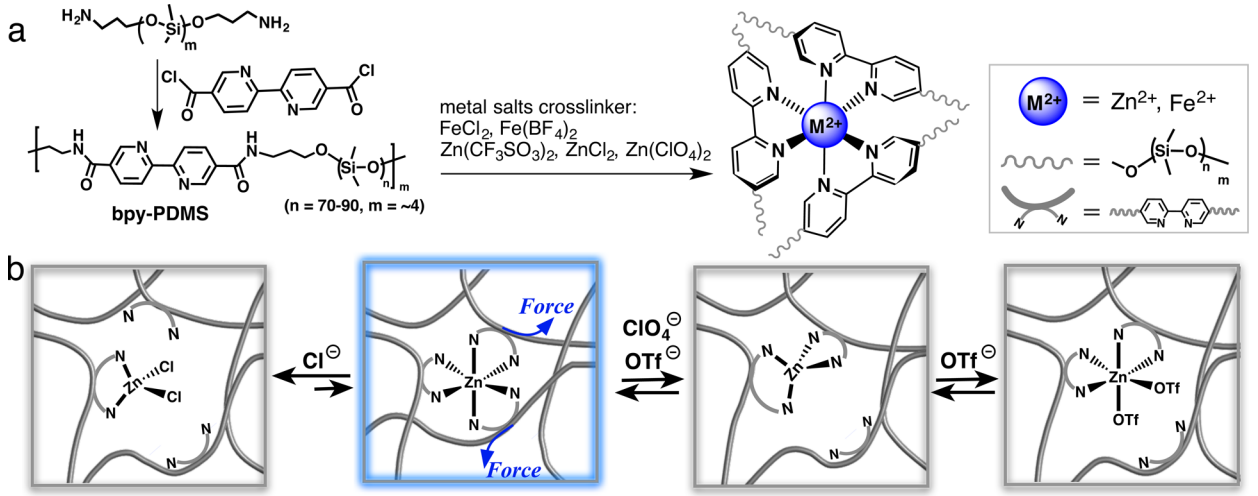

Figure 1. (a) The synthetic route of metal salts cross-linked PDMS. (b) Schematic illustrating the proposed dynamic interactions among metal cations Zn^{2+}, the ligand, and the counteranions in the polymer systems under mechanical stress.

reported a concept to achieve materials with ultrastretchability and self-healing ability through embedding dual-strength dynamic metal−ligand coordination bonds within the soft PDMS polymer backbone.[19] The concept of "dual-strength dynamic bonds" refers to that in the deprotonated 2,6-dicarboxylic amide pyridine (PDCA) chelating ligand, where the coordination geometry around Fe^{3+} metal center is stabilized by the strong coordination through central pyridyl nitrogen along with the flanking either amide oxygen or amide nitrogen anion.

While significant progress has been made in the area of self-healing materials using metal−ligand coordination, applications of materials containing metal−ligand coordination for self-healable electronics remain largely unexplored. Considering that transistors are the basic elements in integrated circuits, we have been developing various strategies for stretchable and self-healable materials for various components in organic field-effect transistors (OFETs). One advantage of introducing metal−ligand coordination bonds into dielectric is that their high polarizability can potentially increase the dielectric constant, which is a desirable feature for gate dielectric materials to reduce operating voltage. While there are few recent reports about self-healing insulating dielectrics for OEFTs, they are either based on inorganic metal oxide,[20] which are incompatible with low-cost printing fabrication methods, or ion-polarized dielectric materials that suffer significant drop of capacitance along with the increase of applied electric-field frequency.[21] Here we describe a new self-healing polymer system, which employs metal−ligand (Fe^{2+}, Zn^{2+}-bipyridine) interactions. To our knowledge, this is the first example of integrating such a system into OFETs as gate insulators. Furthermore, we demonstrate that the transistor electrical stability is closely related to the size of the counteranions of metal ion cross-linkers.

2. RESULTS AND DISCUSSION

2.1. Materials Design and Synthesis. Bipyridine moiety is one of the most widely used neutral ligands in literature, owing to its well-defined coordination geometry with a variety of transition-metal ions.[22] It has been utilized to construct molecular knots,[23,24] metal−organic frameworks (MOF),[25] or the directed self-assembly of peptides.[26] As shown in Figure 1a, our design strategy is to embed bipyridine moieties into a long polydimethylsiloxane (PDMS) chain, which is subsequently cross-linked via metal−ligand coordination between bipyridine moieties and transition-metal ions, Zn^{2+} and Fe^{2+}. While the inherent low T_g of PDMS endows the polymer chains ample motion freedom at room temperature, the choice of metal salts gives us an additional knob to tune the cross-link density and polymer dynamics. The nonpolar PDMS matrix is also important for dielectric application as it reduces ion mobility and ionic effects that may be caused by intentional incorporation of ions. The coordination between the bidentate ligand bipyridine and Fe^{2+} is typically octahedral geometry,[27] with the bond length of N(bipyridyl)-Fe^{2+} being around 1.97 Å.[28] In contrast, Zn^{2+} ions with $3d^{10}$ outer shell electrons, which do not have the ligand-field stabilization effects, show a high degree of flexibility to adopt either tetrahedral or octahedral geometry,[29] depending on the counteranions, solution concentration, and temperature.[30] In an octahedral geometry, the bond length between N(bipyridyl) and Zn^{2+} is around 2.15 Å,[31] which is significantly longer than that of N(bipyridyl)-Fe^{2+}, suggesting that the coordination bond between N(bipyridyl) and Zn^{2+} is more kinetically labile. Moreover, the dynamic coordinating ability of counteranions can help stabilize the complex structure and could potentially serve as energy dissipation sites in bulk materials.[32] Anions with coordinate strength in the order of chloride (Cl^-) ≫ triflate (OTf: $CF_3SO_3^-$) > tetrafluoroborate (BF_4^-), perchlorate-(ClO_4^-) are investigated here.

Bipyridine moieties were incorporated into the PDMS backbone via the equal molar condensation reaction between bis-amine terminated PDMS with 2,2′-bipyridine 5,5′-dicarboxylic acid chloride. Addition of 0.33 equiv of metal salts in the form of $FeCl_2$, $Fe(BF_4)_2$, $ZnCl_2$, $Zn(OTf)_2$, or $Zn(ClO_4)_2$ into the solution of bpy-PDMS (~1 equiv bipyridine moieties) all caused solution gelation, which indicated the metals salt served as effective cross-linkers (Figure 2e). UV−vis absorption spectroscopy was used to monitor metal ion binding stoichiometry (Figure 2a−c). The well-defined isosbestic points in all the UV−vis absorption spectra indicate clean, stoichiometric coordination between bipyridine and Fe^{2+} or Zn^{2+} metal ions. Regardless of the counteranions (Cl^-, BF_4^-), the addition of Fe^{2+} salts to bpy-PDMS solution all generated a

DOI: 10.1021/jacs.6b02428
J. Am. Chem. Soc. 2016, 138, 6020−6027

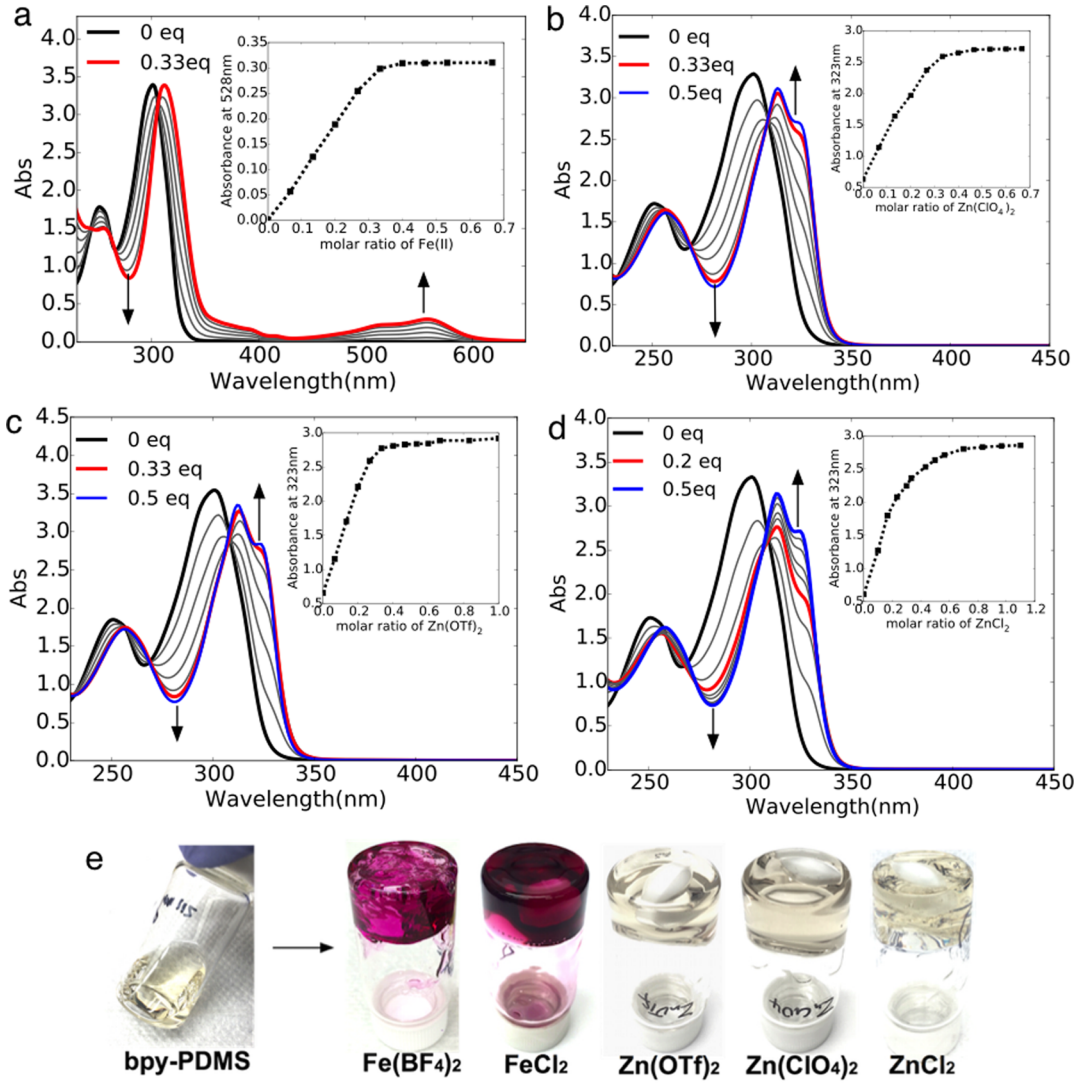

Figure 2. UV−vis absorption spectra acquired upon titration of bpy-PDMS (1×10^{-4} M bipyridine moieties) in CH_2Cl_2 with $FeCl_2$ (a), $Zn(ClO_4)_2$ (b), $Zn(OTf)_2$ (c), and $ZnCl_2$ (d), respectively. The inset in (a) shows the absorption at 528 nm as a function of Fe^{2+}:bpy-PDMS. The insets in (b−d) show the absorption at 323 nm as a function of Zn^{2+}:bipyridine moieties. The interval between each addition is 0.066 equiv. (e) Images showing the gelation formations of bpy-PDMS toluene solution (70 mg/mL, 3 mL) upon the addition of methanol solution of the various metal salts cross-linker (0.18 M/L, 50 μL).

magenta solution with a maximum absorbance at 558 nm, characteristics of the metal-to-ligand charge-transfer electronic transition. The absorption spectra reached saturation in a relative molar ratio of 1:3 Fe^{2+}:bpy-PDMS, consistent with the literature reported octahedral geometry between Fe^{2+} and bidentate ligand bipyridine.[33] In the case of Zn^{2+} salts, the different counteranions have distinct impacts on the coordination geometry. During the titration experiments, the initial addition of Zn^{2+} salts ($ZnCl_2$, $Zn(ClO_4)_2$, $Zn(OTf)_2$) all resulted in a similar change of the UV−vis absorption spectra, with a bathochromic shift of the bipyridine ligand-centered $\pi-\pi^*$ electronic transition. With continuous addition of $Zn(ClO_4)_2$ or $Zn(OTf)_2$ up to ~0.33:1 ratio to bipyridine moieties, the UV−vis absorption spectra reached saturation, which denotes the 1:3 (metal:ligand) octahedral coordination geometry between Zn^{2+} and bipyridine moieties. In the case of $ZnCl_2$, due to the strong coordinating ability of Cl^-, in the reported small molecule models, the coordination geometry between $ZnCl_2$ and bipyridine is generally tetrahedral at room temperature with the two chloride anions tightly bound to the Zn^{2+} center[34] and 1:3 (metal:ligand) octahedral geometry at elevated temperature. However, upon addition of $ZnCl_2$ to bpy-PDMS solution, the viscosity change implied the cross-links among polymer chains. The similarities of changes in the UV−vis spectra upon the initial addition of Zn^{2+} salts ($ZnCl_2$, $Zn(ClO_4)_2$, $Zn(OTf)_2$) also suggested the 1:3 coordination geometry between $ZnCl_2$ and bipyridine moieties. The surprising octahedral coordination geometry between $ZnCl_2$ and bipyridine moieties at room temperature indicates a low reaction activation barrier in the polymer system. The isosbestic points slightly shifted after 0.2 equiv addition of $ZnCl_2$, suggesting the appearance of ordinary tetrahedral coordination geometry (Figure 2d). Thus, the binding geometry in $ZnCl_2$-PDMS is a combination of an initial ~60% 1:3 octahedral geometry with ~40% non-cross-linked tetrahedral coordination (Figure 1b). The distinct coordination geometries are reflected in the polymers' mechanical properties and self-healing ability.

2.2. Mechanical Properties. Polymer films were prepared by solution cast into a Teflon mold and further removal of solvent residue in a vacuum oven over 2 days. The mechanical

DOI: 10.1021/jacs.6b02428
J. Am. Chem. Soc. 2016, 138, 6020−6027

properties of the elastomeric samples are summarized in Table 1. Note that PDMS is a viscous liquid, while bpy-PDMS is a solid due to hydrogen bonding of the amides and $\pi-\pi$ interactions between the bipyridine units. Despite the differences in the dynamic properties of cross-linkers, all polymers showed comparable Young's modulus in the elastic region (E: ~1 MPa within strain <10%). The metal–ligand coordination cross-linkage also displayed hydrolytic stability. Neither weight nor mechanical properties of the polymers were affected after being immersed in water overnight.

Table 1. Summary of Mechanical Properties and Dielectric Constants of Polymers

polymer	E (MPa)[a]	ε (%)[b]	ε_r[c]
bpy-PDMS	1.0 ± 0.1	87 ± 15	2.9
$FeCl_2$-PDMS	0.9 ± 0.2	125 ± 20	3.5
$Fe(BF_4)_2$-PDMS	1.0 ± 0.15	110 ± 16	3.6
$ZnCl_2$-PDMS	1.2 ± 0.21	143 ± 20	3.3
$Zn(ClO_4)_2$-PDMS	1.2 ± 0.15	295 ± 17	3.5
$Zn(OTf)_2$-PDMS	1.1 ± 0.2	310 ± 15	3.5

[a]Young's modulus, calculated from the initial slope of stress–strain curves (within 10% strain). [b]Ultimate tensile strain (displacement rate: 5 mm/min). [c]Dielectric constant.

To further correlate the kinetic stability of the cross-linkers with dynamic properties of the polymer, cyclic stress–strain hysteresis and stress relaxation studies were performed. From the cyclic stress–strain experiments, the functionalized PDMS demonstrated different extent of hysteresis between loading and unloading curves (Figure 3a). The extent of hysteresis was consistent with the stress relaxation experiments (Figure 3b) and tensile stress variation with displacement rates (Figure S6). With Zn^{2+} as the cross-linkers, the polymers exhibited much larger hysteresis and faster stress relaxation rate compared to those with Fe^{2+} as the cross-linkers. The Zn^{2+} cross-linkers' superior ability to dissipate energy upon mechanical stress is owing to two factors: First, Zn^{2+}-N(bipyridyl) bond is more kinetically labile than that of Fe^{2+}-N(bipyridyl); and second, the aptitude of Zn^{2+} ions to adopt both octahedral and tetrahedral geometries offers another avenue to minimize stress concentration. Notably, the stress relaxation rate is also related to the choices of counteranions. The stress relaxation rates found in polymers in the order of $Zn(OTf)_2$-PDMS > $Zn(ClO_4)_2$-PDMS > $ZnCl_2$-PDMS suggest that the degree of polymer dynamics follows the same order. Based on this, we propose that the counteranions with different coordinating abilities might also affect the coordination geometry, which is then closely related to the polymer dynamics. The proposed dynamic coordination geometry under mechanical stress is illustrated in Figure 1b. After the dissociation of Zn^{2+}-N(bipyridyl) bond, it is likely that the weakly coordinating triflate anions would temporarily occupy the empty coordination sites to stabilize the polymer network. In contrast, more

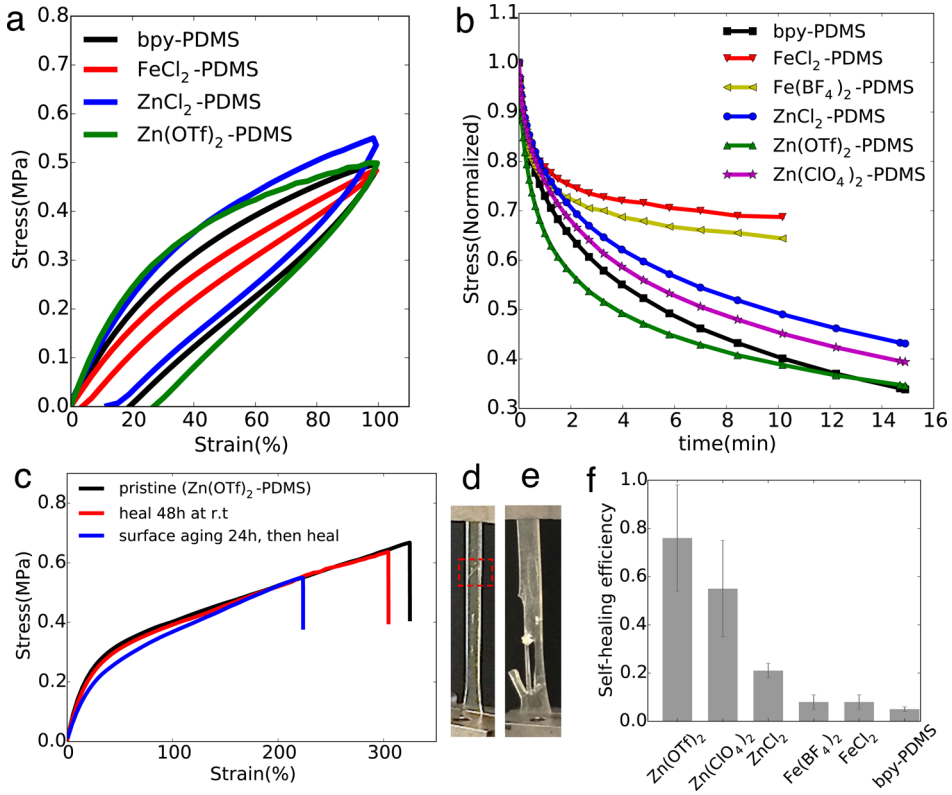

Figure 3. (a) The stress–strain curves of polymers bpy-PDMS, $FeCl_2$-PDMS, $ZnCl_2$ and $Zn(OTf)_2$-PDMS, showing different degrees of hysteresis (displacement rate: 5 mm/min). (b) Stress relaxation data for all polymers. (c) Self-healing test for $Zn(OTf)_2$-PDMS polymer at ambient condition without any intervention. (d, e) Images showing the self-healed $Zn(OTf)_2$-PDMS polymer film under tensile stress (>250% strain): (d) the pristine film was cut into two pieces, then subjected to self-heal, and the joining edge of the cut films is highlighted in red dot box; (e) the pristine film was ruptured into two pieces under tensile stress, and the ruptured surface was then gently pushed back together and subjected to self-heal. This image clearly shows parts of the ruptured surface were completely healed to withstand the tensile stress. (f) The bar graph summarizing the self-healing efficiencies of all polymers at ambient condition after 48 h.

DOI: 10.1021/jacs.6b02428
J. Am. Chem. Soc. 2016, 138, 6020–6027

labile anions ClO_4^- do not have the ability to coordinate, while strongly coordinating anions Cl^- would block the coordination sites and disrupt the polymer network. More detailed investigation of mechanical properties and their correlation to molecular structures is not a focus of this report and will be a subject for future study. Lastly, though the uncross-linked bpy-PDMS polymer also showed large hysteresis and fast stress relaxation rate, this was more of a phenomenon of thermoplastic deformation from irreversible interchain slipping.

To test the self-healing ability, polymer films were cut through completely with a razor blade, and the cut interfaces were gently pushed together for a few seconds, then left to allow self-healing at room temperature (rt) for 2 days. The polymers' self-healing efficiency is defined as the fracture strain of healed sample to that of the pristine sample in stress−strain experiments. Figure 3c shows the strain and stress at break of pristine and healed $Zn(OTf)_2$-PDMS films, with healing efficiency of 76 ± 22%. Notably, the healing efficiencies were not significantly affected by surface aging effects. With the cut surfaces of $Zn(OTf)_2$-PDMS film exposed at ambient condition for 24 h, the polymer film still retained a self-healing efficiency of ~60%. Lower healing efficiencies of 55 ± 21% and 21 ± 3% were observed for $Zn(ClO_4)_2$-PDMS and $ZnCl_2$-PDMS (Figure 3f). Fe^{2+} cross-linker polymers showed insignificant amount of self-healing ability at rt due to the kinetically inert Fe^{2+}-N(bipyridyl) coordination at rt.[35] The trend of polymers' self-healing efficiencies follows the order of the dynamics of coordination geometries on the molecular level, i.e., a higher degree of the cross-linker dynamics endows polymers better self-healing ability. Not surprisingly, the Fe^{2+} cross-linked polymers were completely healable upon heating at 90 °C for a few hours, owing to mutual contributions of higher degree of polymer chain mobility and more labile Fe^{2+}-N(bipyridyl) coordination at higher temperature.[35] Furthermore, the uncross-linked bpy-PDMS polymer displayed minimal self-healing ability at rt, verifying that the self-healing in the metal ions cross-linked polymers was mainly due to the metal−ligand coordination.

2.3. Electrical Properties. Electrical stability of the transistor elements is crucial in integrated organic circuits.[36] In OFETs, the presence of mobile ions in the dielectric might result in hysteresis effects in the transfer characteristics (I_{DS} vs V_{GS}), indicating an electrical instability.[37] Polymer dielectrics are often hosts for mobile ions, the source of which may potentially come from cross-linking reagents or salt impurities incorporated during material synthesis and handling. The hysteresis due to mobile ionic impurities in OFETs has been observed in poly(vinyl alcohol),[38] fluorinated elastomers,[39] and thermoplastic polyurethane gate dielectrics.[40] As metal ions were deliberately added into our materials to serve as cross-linkers, it was imperative to study the presence of ionic effects in the materials as gate dielectrics.

A metal−insulator−metal (MIM) device structure was used for capacitance measurements. The capacitance values of metal ions cross-linked PDMS all demonstrated stability over a wide range of operating frequencies from 20 to 10^5 Hz, as shown in Figure 4. As ionic polarization often occurs at low frequencies, an upper bound on the capacitance was obtained by quasistatic capacitance measurements via the time response of a resistor−capacitor (RC) circuit containing a reference resistor of about 500 MΩ.[39] The capacitance values extracted using this method correspond to a frequency window of 0.05 Hz < f < 1 Hz and are similar to the value at much higher frequencies, indicating

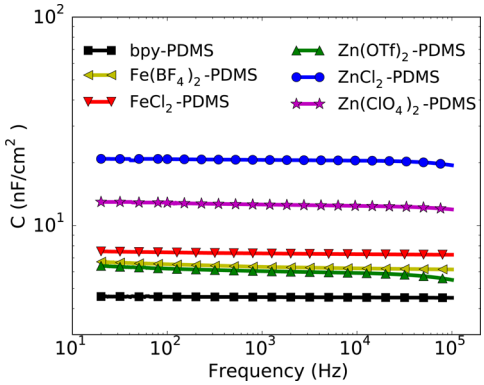

Figure 4. Capacitance versus frequency measured for various functionalized PDMS (bpy-PDMS: 550 nm; $Fe(BF_4)_2$-PDMS: 490 nm; $FeCl_2$-PDMS: 386 nm; $Zn(OTf)_2$-PDMS: 470 nm; $ZnCl_2$-PDMS: 138 nm; $Zn(ClO_4)_2$-PDMS: 238 nm).

no ionic effects in dielectric behavior in these polymer systems. The low ionic mobility in the functionalized PDMS elastomers is related to both the nonpolar siloxane matrix and the stable coordination between bipyridine moieties and the metal salts. The dielectric constants of metal ions cross-linked PDMS are summarized in Table 1. The addition of metal ions has effectively increased the material's dielectric constant compared to the pure bipyridyl-bridged bpy-PDMS. This is desirable as an increase of the dielectric constant of insulating material could lower the operating voltage of transistors.

To test the feasibility of the metal ions cross-linked PDMS as gate insulators, OFETs were fabricated using either p- or n-type polymeric semiconductor in a bottom-contact top-gate device geometry with the dielectric directly coated onto the semiconductor film (Figure 5a). The p-type semiconductors used here are a series of previously reported donor−acceptor tetrathienoacene-diketopyrrolopyrrole (TTA-DPP)-based polymers (P1−P3, Figure 5b) with different side chains and backbone spacers,[41] while n-type semiconducting channel layer uses poly(naphthalenediimide-bithiophene) (P(NDI2OD-T2)) polymer (N1).[42] The effects of mobile ions in the dielectrics were investigated through the hysteresis from the cyclic transfer characteristics (I_D vs V_G), where I_D depends on the sweep direction of V_G. As shown in Figure 5c,e (Figures S9 and S10 in SI), p-type polymeric semiconductor-based OFETs with $FeCl_2$-PDMS or $ZnCl_2$-PDMS dielectric layer all exhibited ideal, hysteresis-free transfer characteristics. In contrast, with $Fe(BF_4)_2$-PDMS, $Zn(ClO_4)_2$-PDMS, or $Zn(OTf)_2$-PDMS dielectrics, the p-type OFETs all demonstrated prominent hysteresis phenomena with a higher back sweep current (the sweep from on to off). This is explained by the mobile anions drifting in the dielectrics when a gate field is applied (Figure 5i−k; Figures S11 and S12 in SI). Upon applying an "on" gate voltage (negative bias), the anions move toward the dielectric/semiconductor interface. When V_G is swept back, initially, the anions stay localized at the interface increasing the effective electric field, causing therefore higher back sweep current, i.e., current hysteresis. The hysteresis phenomena also increase with slower gate voltage sweep rate, which is consistent with the explanation that a higher number of mobile anions accumulate close to the dielectric/semiconductor interface when the on-voltage bias is applied for a longer time. It is also apparent that dielectrics with larger-sized counteranions displayed wider hysteresis in the transfer characteristics. With the addition of

DOI: 10.1021/jacs.6b02428
J. Am. Chem. Soc. 2016, 138, 6020−6027

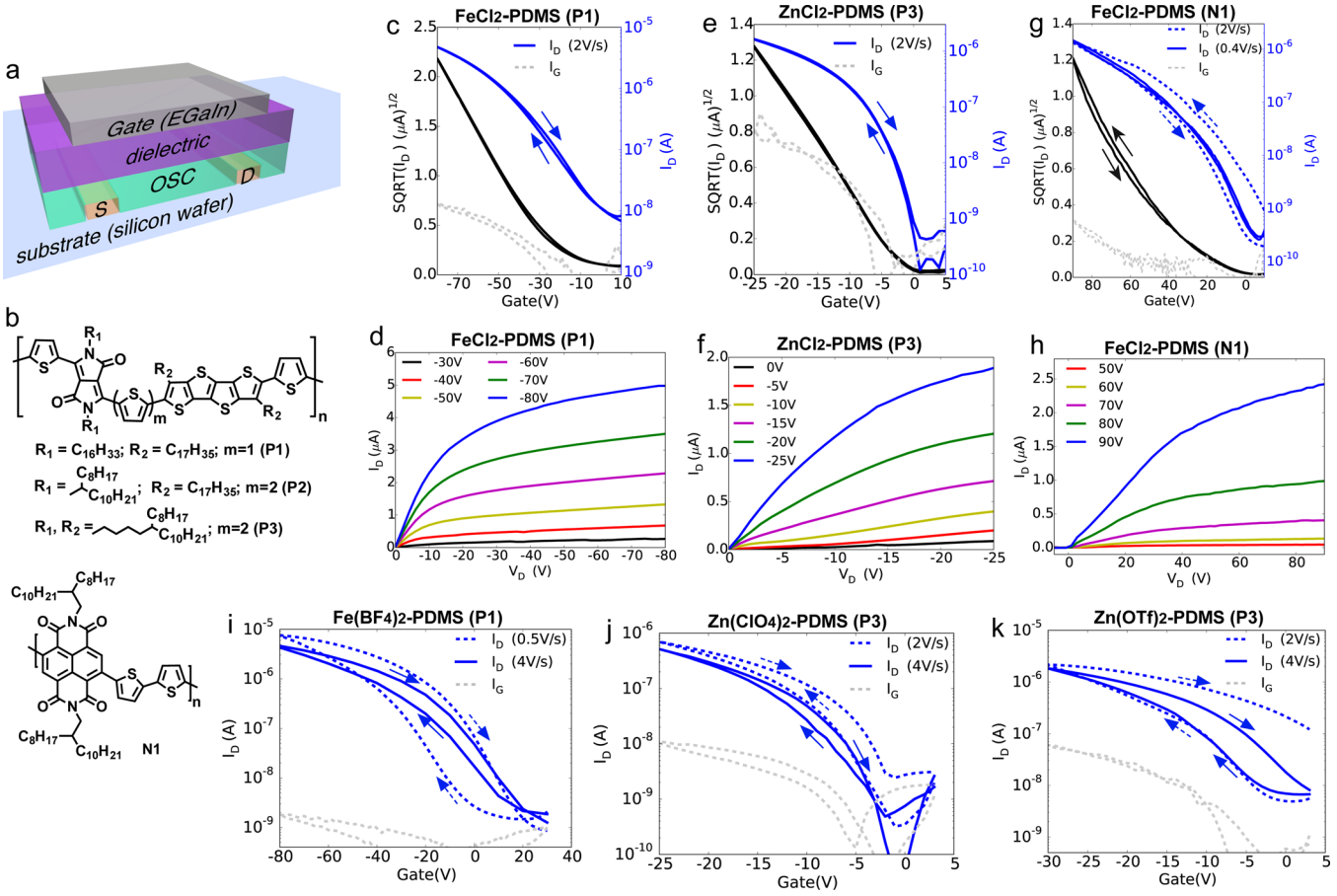

Figure 5. (a) Schematic of the OFET device structure in a top-gate bottom-contact geometry on rigid substrate (silicon wafer). (b) Chemical structures of P-type (P1−P3) and N-type (N1) organic semiconducting (OSC) polymers used here. (c−k) Transfer (I_D versus V_G) and output curve characteristics of OFETs with channel width of 4000 μm (arrows denote gate bias sweep directions and the gate voltage scan rate is normalized to that of 1um thickness): (c) Transfer curve and (d) output curve of P1, with 5.5 μm thick $FeCl_2$-PDMS as dielectrics (C: 0.56 nF/cm^2, channel L: 50 μm). (e) Transfer curve and (f) output curve of P3, with 1.2 μm thick $ZnCl_2$-PDMS as dielectrics (C: 2.4 nF/cm^2, channel L: 100 μm). (g) Transfer curve and (h) output curve of N1, with 5.5 μm thick $FeCl_2$-PDMS as dielectrics (C: 0.56 nF/cm^2, channel L: 50 μm) (i) Transfer curve of P1, with 6 μm thick $Fe(BF_4)_2$-PDMS as dielectrics (C: 0.53 nF/cm^2, channel L: 50 μm). (j) Transfer curve of P3, with 1.4 μm thick $Zn(ClO_4)_2$-PDMS as dielectrics (C: 2.2nF/cm^2, channel L: 200 μm). (k) Transfer curve of P3 with 1.5 μm thick $Zn(OTf)_2$-PDMS as dielectrics (C: 2.1nF/cm^2, channel L: 200 μm).

Table 2. Summary of OFETs Electrical Performances of Various Semiconductors (P1−P3 and N1), Using $FeCl_2$-PDMS or $ZnCl_2$-PDMS as Dielectrics[a]

	$FeCl_2$-PDMS					$ZnCl_2$-PDMS				
OSC	d[b] (μm)	C[c] (nF/cm^2)	μ (cm^2/V·s)	V_{th}	on/off	d (μm)	C (nF/cm^2)	μ (cm^2/V·s)	V_{th}	on/off
P1	3.5	0.88	0.19 ± 0.03	−15 ± 2	5.9 × 10^3	5	0.58	0.17 ± 0.03	−21 ± 4	3.2 × 10^3
	5.5	0.56	0.16 ± 0.02	−18 ± 4	2.1 × 10^3					
P2	3.5	0.88	0.18 ± 0.02	7 ± 3	4.4 × 10^3	3	0.97	0.2 ± 0.02	1.1 ± 0.6	2.1 × 10^3
P3	3.5	0.88	0.35 ± 0.1	2.5 ± 5	1.3 × 10^3	1.2	2.4	0.29 ± 0.06	−2 ± 2	1.2 × 10^4
N1	5.5	0.56	0.11 ± 0.04	27 ± 10	5.3 × 10^3	1.2	2.4	0.14 ± 0.03	1.2 ± 5	2.7 × 10^3

[a]Channel W: 4000 μm; L: 50 μm. [b]Dielectric thickness. [c]Dielectric capacitance value.

metal salts as the cross-linkers for the dielectric polymer matrix, the metal cations (Fe^{2+}, Zn^{2+}) are affixed to the polymer backbone via coordination bonds, and the counteranions with a smaller size would result in stronger ion pairs, which can inhibit mobile anions drifting under electric bias. This explains the absence of hysteresis in $FeCl_2$-PDMS or $ZnCl_2$-PDMS dielectrics with the small-sized counteranion Cl^- and also provides important guidance for future dielectric material design.

Similar hysteresis phenomena were also observed in n-type polymeric semiconductor-based OFETs. With $Zn(OTf)_2$-PDMS dielectrics (Figure S12c in SI), the OFETs displayed a higher back sweep current. Upon applying an "on" gate voltage (positive bias), the anions move away from the semiconductor, leaving the positively charged polymer backbone close to the dielectric/semiconductor interface. When V_G is swept back, the positively charged polymer backbone increases the effective gate field and causes higher back sweep current, i.e., current hysteresis. With $FeCl_2$-PDMS (Figure 5g) or $ZnCl_2$-PDMS

DOI: 10.1021/jacs.6b02428
J. Am. Chem. Soc. 2016, 138, 6020−6027

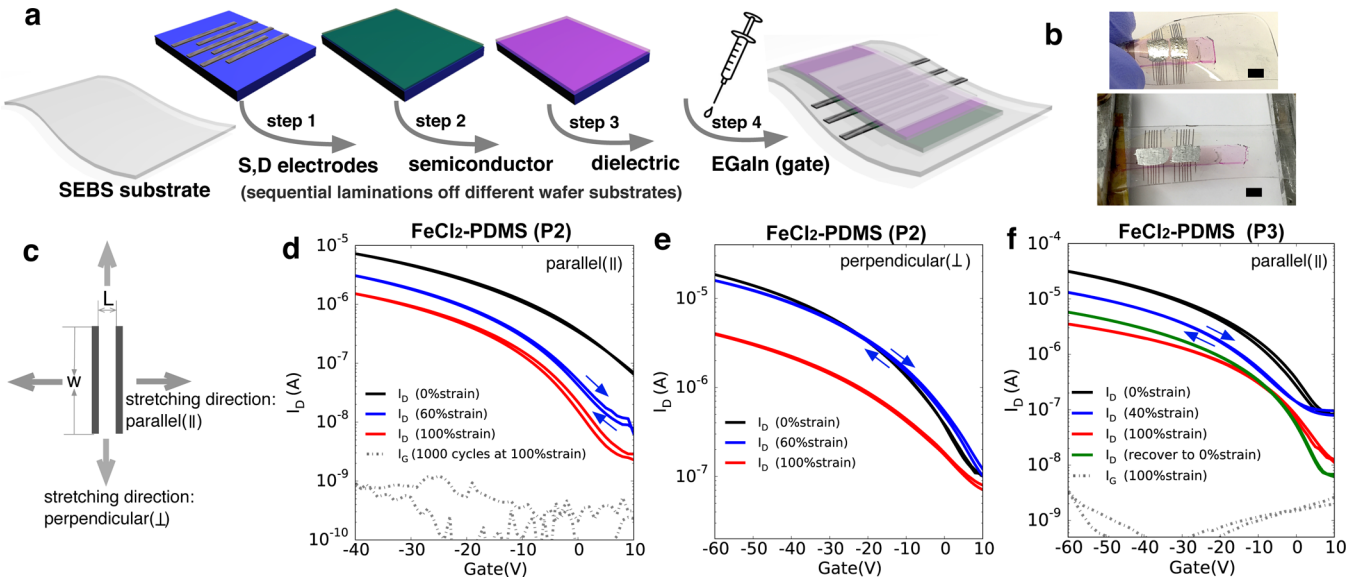

Figure 6. (a) Fabrication flow of fully stretchable transistors. (b) Images of the flexible device at 0% (top) and 100% (bottom) tensile strain, scale bar: 4 mm. (c) Diagram depicting the stretching direction. (d–f) Transfer curve (I_D versus V_G) characteristics of fully stretchable transistors of P2 (d, e) and P3 (f), with 3.5 μm thick $FeCl_2$-PDMS as dielectrics (C: 0.85 nF/cm^2, channel W: 4000 μm, L: 50 μm) at various tensile strain.

(Figure S10d in SI) as dielectrics, the OFETs displayed a lower back sweep current hysteresis dominated by the trapping of charge carriers at the semiconductor–dielectrics interface. With a slower gate voltage sweep rate, the lower back sweep current hysteresis can be eliminated in the case of $FeCl_2$-PDMS dielectrics, suggesting that the electron traps are filled. This further proves the absence of mobile anions drifting in $FeCl_2$-PDMS and $ZnCl_2$-PDMS dielectrics (Table 2).

Encouraged by the stable electrical performance of metal salts cross-linked elastomers containing Cl^- anions, we then fabricated fully stretchable transistors with $FeCl_2$-PDMS as dielectrics and P2 or P3 as p-type polymeric semiconductors. Bottom contact, top gate devices were fabricated using sequential lamination transfers from rigid silicon substrates according to a procedure modified from our previously published work.[43] Briefly, unsorted CNTs were spray coated onto an octadecyltrimethoxysilane (OTMS)-treated wafer,[44] then followed by patterning and lamination onto hydrogenated styrene butadiene block copolymer (SEBS) substrates to form source and drain electrodes. Polymeric semiconductors and dielectrics spin-coated on separate OTMS-treated wafers were sequentially transferred onto the SEBS substrate (Figure 6a). The transistor device was completed via the application of EGaIn liquid metal on top as the gate electrode. Representative transfer curves with P2 or P3 as semiconductors are shown in Figure 6d–f, which exhibits ideal, hysteresis-free transfer characteristics. Strain dependence of the transistor performance was evaluated by stretching the substrate both parallel and perpendicular to the charge transport direction. Within both tested strain range and directions, the fully stretchable transistors retained good transfer characteristics, suggesting that the semiconductor and dielectrics remain a good contact interface when the device is under mechanical deformation. Though the mobility of the transistor decreases under strain, this is intrinsic to the properties of polymeric semiconductors used here, which form cracks under strain and thus exhibit a drop of mobility. Notably, the gate leakage current remains under 1 nA even after 1000 cycles of strain up to 100% (Figure 6d), indicating the mechanical robustness of the $FeCl_2$-PDMS dielectric film.

3. CONCLUSIONS

In summary, we have demonstrated a new class of metal salts cross-linked elastomers based on the metal–ligand coordination between transition-metal ions (Fe^{2+}, Zn^{2+}) and bipyridine moieties incorporated in the PDMS backbone. The identity of metal cations and their counteranions determines the coordination geometry and bond strength and is used to further influence the bulk polymer's mechanical properties and electrical performances. The polymers' self-healing ability is primarily determined by the kinetic lability of the metal–ligand coordination bonds. We found that PDMS polymers cross-linked with zinc salts ($Zn(OTf)_2$, $Zn(ClO_4)_2$) exhibited much better self-healing abilities than those of polymers cross-linked with iron salts. Moreover, surface aging has minimal effects on self-healing efficiency. Addition of metal salts as polymer cross-linkers also serves as an effective strategy to increase the materials' dielectric constants, while maintaining the stable capacitance without introducing undesirable ionic effects. When the metal salts cross-linked PDMS integrated into OFETs as a dielectric layer, the electrical stability of the transistor is closely related to the ion pair strength of the metal salts. Transistors with $FeCl_2$-PDMS or $ZnCl_2$-PDMS as dielectrics demonstrated ideal, hysteresis-free transfer characteristics, owing to that the strong columbic interaction between metal ion and small Cl^- anion can prevent mobile anions drifting under gate bias. Fully stretchable transistors with $FeCl_2$-PDMS dielectrics also displayed stable transfer characteristics and low gate leakage current after 1000 cycles at 100% strain. The mechanical robustness and stable electrical performance proved that metal salts cross-linked nonpolar PDMS are suitable for applications in stretchable electronics, for potential applications in wearable sensors and electronic skins. Similar coordination chemistry could be potentially expanded into other polymer matrices to allow additional tunabilities. We conclude that to obtain polymer dielectrics possessing both autonomous self-healing ability and stable electrical performances, utilizing high-

DOI: 10.1021/jacs.6b02428
J. Am. Chem. Soc. 2016, 138, 6020–6027

coordinate metal ions which can form flexible, labile coordination geometry with ligands and strong interaction with the counteranions is a desirable strategy.

■ ASSOCIATED CONTENT

Supporting Information

The Supporting Information is available free of charge on the ACS Publications website at DOI: 10.1021/jacs.6b02428.

Synthesis, UV−vis absorption titration, TGA, DSC, mechanical test, device fabrications, additional transistors transfer characteristics, SAXS data (PDF)

■ AUTHOR INFORMATION

Corresponding Author

*zbao@stanford.edu

Notes

The authors declare no competing financial interest.

■ ACKNOWLEDGMENTS

This work was supported by Samsung Electronics and Air Force Office of Scientific Research (FA9550-15-1-0106). Y.-L.R. thanks the Canadian Natural Science and Engineering Research Council (NSERC) Postdoctoral Fellowship. R.P. is grateful to Generalitat de Catalunya for a Beatriu de Pinós, Marie Curie COFUND fellowship. F.L. thanks the Swiss National Science Foundation for an Early Mobility Postdoc grant. Portions of this research were carried out at the Stanford Synchrotron Radiation Lightsource, a Directorate of SLAC National Accelerator Laboratory and an Office of Science User Facility operated for the U.S. Department of Energy Office of Science by Stanford University. The beam line 4−2 is part of the SSRL Structural Molecular Biology Program which is supported by the DOE Office of Biological and Environmental Research, and by the National Institutes of Health, National Institute of General Medical Sciences (including P41GM103393) and the National Center for Research Resources (P41RR001209). The contents of this publication are solely the responsibility of the authors and do not necessarily represent the official views of NIGMS, NCRR or NIH.

■ REFERENCES

(1) Rogers, J. A.; Someya, T.; Huang, Y. *Science* **2010**, *327*, 1603.
(2) Park, S.; Vosguerichian, M.; Bao, Z. *Nanoscale* **2013**, *5*, 1727.
(3) Sekitani, T.; Someya, T. *Adv. Mater.* **2010**, *22*, 2228.
(4) Ko, H.; Kapadia, R.; Takei, K.; Takahashi, T.; Zhang, X.; Javey, A. *Nanotechnology* **2012**, *23*, 344001.
(5) Kim, D.-H.; Ghaffari, R.; Lu, N.; Rogers, J. A. *Annu. Rev. Biomed. Eng.* **2012**, *14*, 113.
(6) Arias, A. C.; MacKenzie, J. D.; McCulloch, I.; Rivnay, J.; Salleo, A. *Chem. Rev.* **2010**, *110*, 3.
(7) Irimia-Vladu, M.; Głowacki, E. D.; Voss, G.; Bauer, S.; Sariciftci, N. S. *Mater. Today* **2012**, *15*, 340.
(8) Bettinger, C. J.; Bao, Z. *Adv. Mater.* **2010**, *22*, 651.
(9) Hammock, M. L.; Chortos, A.; Tee, B. C. K.; Tok, J. B. H.; Bao, Z. *Adv. Mater.* **2013**, *25*, 5997.
(10) Rivnay, J.; Owens, R. M.; Malliaras, G. G. *Chem. Mater.* **2014**, *26*, 679.
(11) Tee, B. C.-K.; Wang, C.; Allen, R.; Bao, Z. *Nat. Nanotechnol.* **2012**, *7*, 825.
(12) Chen, P.; Li, Q.; Grindy, S.; Holten-Andersen, N. *J. Am. Chem. Soc.* **2015**, *137*, 11590.
(13) Wang, C.; Wu, H.; Chen, Z.; McDowell, M. T.; Cui, Y.; Bao, Z. *Nat. Chem.* **2013**, *5*, 1042.
(14) Yang, Y.; Urban, M. W. *Chem. Soc. Rev.* **2013**, *42*, 7446.
(15) Williams, K. A.; Boydston, A. J.; Bielawski, C. W. *J. R. Soc., Interface* **2007**, *4*, 359.
(16) Burnworth, M.; Tang, L.; Kumpfer, J. R.; Duncan, A. J.; Beyer, F. L.; Fiore, G. L.; Rowan, S. J.; Weder, C. *Nature* **2011**, *472*, 334.
(17) Holten-Andersen, N.; Harrington, M. J.; Birkedal, H.; Lee, B. P.; Messersmith, P. B.; Lee, K. Y. C.; Waite, J. H. *Proc. Natl. Acad. Sci. U. S. A.* **2011**, *108*, 2651.
(18) Mozhdehi, D.; Ayala, S.; Cromwell, O. R.; Guan, Z. *J. Am. Chem. Soc.* **2014**, *136*, 16128.
(19) Li, C.-H.; Wang, C.; Keplinger, C.; Zuo, J.-L.; Jin, L.; Sun, Y.; Zheng, P.; Cao, Y.; Lissel, F.; Linder, C.; You, X.-Z.; Bao, Z. *Nat. Chem.* **2016**, 2492.
(20) Lu, C.-C.; Lin, Y.-C.; Yeh, C.-H.; Huang, J.-C.; Chiu, P.-W. *ACS Nano* **2012**, *6*, 4469.
(21) Huang, W.; Besar, K.; Zhang, Y.; Yang, S.; Wiedman, G.; Liu, Y.; Guo, W.; Song, J.; Hemker, K.; Hristova, K.; Kymissis, I. J.; Katz, H. E. *Adv. Funct. Mater.* **2015**, *24*, 3745.
(22) Kaes, C.; Katz, A.; Hosseini, M. W. *Chem. Rev.* **2000**, *100*, 3553.
(23) Ayme, J.-F.; Beves, J. E.; Campbell, C. J.; Gil-Ramírez, G.; Leigh, D. a.; Stephens, A. J. *J. Am. Chem. Soc.* **2015**, *137*, 9812.
(24) Guo, J.; Mayers, P. C.; Breault, G. A.; Hunter, C. A. *Nat. Chem.* **2010**, *2*, 218.
(25) Ye, B. H.; Tong, M. L.; Chen, X. M. *Coord. Chem. Rev.* **2005**, *249*, 545.
(26) Przybyla, D. E.; Chmielewski, J. *J. Am. Chem. Soc.* **2008**, *130*, 12610.
(27) Przybyla, D. E.; Chmielewski, J. *J. Am. Chem. Soc.* **2010**, *132*, 7866.
(28) Decurtins, S.; Schmalle, H. W.; Schneuwly, P.; Oswald, H. R. *Inorg. Chem.* **1993**, *32*, 1888.
(29) Sénéchal, K.; Maury, O.; Le Bozec, H.; Ledoux, I.; Zyss, J. *J. Am. Chem. Soc.* **2002**, *124*, 4560.
(30) Younes, A. H.; Zhang, L.; Clark, R. J.; Zhu, L. *J. Org. Chem.* **2009**, *74*, 8761.
(31) Chen, X. M.; Wang, R. Q.; Yu, X. L. *Acta Crystallogr., Sect. C: Cryst. Struct. Commun.* **1995**, *51*, 1545.
(32) Kean, Z. S.; Hawk, J. L.; Lin, S.; Zhao, X.; Sijbesma, R. P.; Craig, S. L. *Adv. Mater.* **2014**, *26*, 6013.
(33) Shankar, S.; Lahav, M.; van der Boom, M. E. *J. Am. Chem. Soc.* **2015**, *137*, 4050.
(34) Khan, M. A.; Tuck, D. G. *Acta Crystallogr., Sect. C: Cryst. Struct. Commun.* **1984**, *40*, 60.
(35) Akhuli, B.; Cera, L.; Jana, B.; Saha, S.; Schalley, C. a; Ghosh, P. *Inorg. Chem.* **2015**, *54*, 4231.
(36) Facchetti, A.; Yoon, M.-H.; Marks, T. J. *Adv. Mater.* **2005**, *17*, 1705.
(37) Egginger, M.; Bauer, S.; Schwödiauer, R.; Neugebauer, H.; Sariciftci, N. S. *Monatsh. Chem.* **2009**, *140*, 735.
(38) Egginger, M.; Irimia-Vladu, M.; Schwödiauer, R.; Tanda, a.; Frischauf, I.; Bauer, S.; Sariciftci, N. S. *Adv. Mater.* **2008**, *20*, 1018.
(39) Wang, C.; Lee, W.-Y.; Kong, D.; Pfattner, R.; Schweicher, G.; Nakajima, R.; Lu, C.; Mei, J.; Lee, T. H.; Wu, H.-C.; Lopez, J.; Diao, Y.; Gu, X.; Himmelberger, S.; Niu, W.; Matthews, J. R.; He, M.; Salleo, A.; Nishi, Y.; Bao, Z. *Sci. Rep.* **2015**, *5*, 17849.
(40) Chortos, A.; Koleilat, G. I.; Pfattner, R.; Kong, D.; Lin, P.; Nur, R.; Lei, T.; Wang, H.; Liu, N.; Lai, Y.-C.; Kim, M.-G.; Chung, J. W.; Lee, S.; Bao, Z. *Adv. Mater.* **2015**, DOI: 10.1002/adma.201501828.
(41) Matthews, J. R.; Niu, W.; Tandia, A.; Wallace, A. L.; Hu, J.; Lee, W. Y.; Giri, G.; Mannsfeld, S. C. B.; Xie, Y.; Cai, S.; Fong, H. H.; Bao, Z.; He, M. *Chem. Mater.* **2013**, *25*, 782.
(42) (a) Yan, H.; Chen, Z.; Zheng, Y.; Newman, C.; Quinn, J. R.; Dötz, F.; Kastler, M.; Facchetti, A. *Nature* **2009**, *457*, 679. (b) Kurosawa, T.; Chiu, Y.-C.; Zhou, Y.; Gu, X.; Chen, W.-C.; Bao, Z. *Adv. Funct. Mater.* **2016**, *26*, 1261.
(43) Chortos, A.; Lim, J.; To, J. W. F.; Vosgueritchian, M.; Dusseault, T. J.; Kim, T. H.; Hwang, S.; Bao, Z. *Adv. Mater.* **2014**, *26*, 4253.
(44) Ito, Y.; Virkar, A. A.; Mannsfeld, S.; Oh, J. H.; Toney, M.; Locklin, J.; Bao, Z. *J. Am. Chem. Soc.* **2009**, *131*, 9396.

DOI: 10.1021/jacs.6b02428
J. Am. Chem. Soc. 2016, 138, 6020−6027